Understanding climate change over the southwestern Mediterranean using high-resolution simulations

Alexandre Tuel[1] · Suchul Kang[1] · Elfatih A. B. Eltahir[1]

Abstract

The severe wintertime precipitation decline projected by global climate models (GCMs) over the Southwestern Mediterranean makes this region a major climate change hotspot. Here, we evaluate the performance of the MIT Regional Climate Model (MRCM) in simulating seasonal and inter-annual regional climatic features over Northwestern Africa and the Iberian Peninsula (NWAIP), and develop and interpret regional climate change projections over the same region under the RCP4.5 and 8.5 scenarios, at a resolution of 12 km, driven by three carefully selected GCMs. MRCM succeeds in correctly capturing the spatio-temporal patterns of precipitation when forced by ERA-Interim reanalysis data. In addition to substantial year-round warming, the MRCM ensemble projects a significant decline in precipitation during winter and spring under continued anthropogenic forcing. Even with significant climate change mitigation, the drying is relatively large, with an average of − 34% in precipitation over Morocco's three main watersheds during spring, and − 22% during winter. Projections for the Iberian Peninsula are less severe, though drying trends are still robust. The consistency of the precipitation projections is discussed in the light of physical mechanisms acting at the regional scale. Being located downwind of a large desert, the region is particularly vulnerable to the changes in circulation projected by global models. The latter will advect dry air from the Sahara, which will suppress precipitation. The local topography also contributes to these trends. Overall, our results elucidate the physical processes responsible for winter and spring drying in the southwestern Mediterranean.

1 Introduction

Among all land regions, the Mediterranean has long been recognized as a major climate change hotspot for the coming century (Giorgi and Lionello 2008; Diffenbaugh and Giorgi 2012). The vast majority of climate models point to a shift towards significantly drier conditions during winter and spring, when southern Mediterranean countries receive the bulk of their annual precipitation. Coupled Model Intercomparison Project phase 5 (CMIP5, Taylor et al. 2012) Global Climate Models (GCMs) project that annual precipitation decreases could locally reach 40% under a business-as-usual scenario (RCP8.5, IPCC 2013) (Zappa et al. 2015).

If realized, this would severely affect the habitability and stability of the basin in the next decades (Dubrovsky et al. 2014). These changes are bound to have enormous impacts on the regional economy, very dependent on the agricultural sector and water resources. This is particularly true for Morocco and southern Spain (Balaghi et al. 2012), where the decline in precipitation will be highest across the whole Mediterranean (Tuel and Eltahir 2020).

However, precipitation over Morocco and Andalusia is strongly variable in space and time, and largely determined by the complex topography, with large maxima over the Rif and Atlas Range peaks, and over Spain's coastal plains and Sierra Nevada (Figs. 1a, 3a). Because of their coarse resolution, GCMs are unable to reproduce these fine-scale, critical details (Fig. S1), making the case for the downscaling of climate projections (Gao et al. 2006). Climate data records are very sparse in this area, notably in the mountain regions, and consequently statistical downscaling is hardly an option as it requires long series of observations for calibration. Regional Climate Models (RCMs), on the other hand, are well-suited when reliable records are not available. They can provide more detailed physical insights into the future climate of a

✉ Alexandre Tuel
atuel@mit.edu

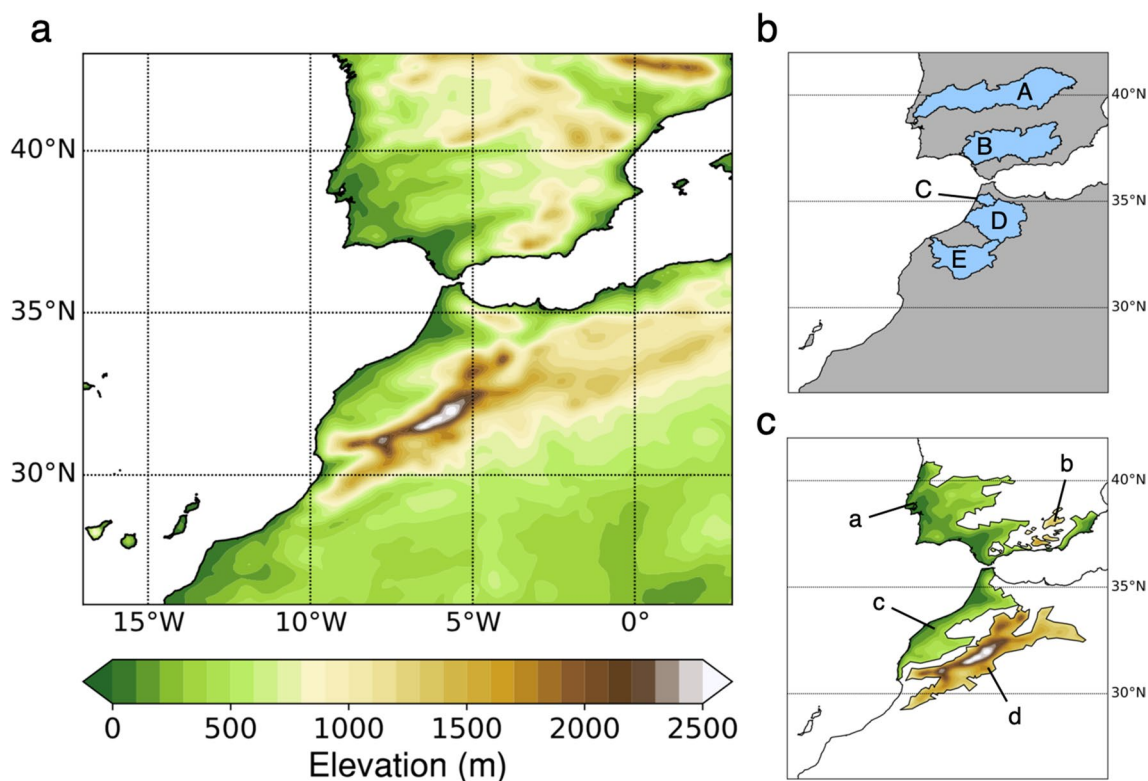1 Ralph M. Parsons Laboratory, Massachusetts Institute of Technology, Cambridge, MA 02139, USA

Fig. 1 a MRCM simulation domain and topography. **b** Sub-regions used for regional analysis of precipitation projections: **A** Tajo, **B** Guadalquivir, **C** Loukkos, **D** Sebou and **E** Oum-Er-Rbia watersheds. **c** Sub-regions used for regional analysis of temperature projections: **a** Iberian coastal plain, **b** Sierra Nevada, **c** Moroccan coastal plain and **d** Atlas Range. **a**, **c** are defined by altitude < 500 m and **b**, **d** by altitude > 1200 m at the MRCM resolution

region, down to scales that are relevant for water management applications. RCMs have notably been shown to bring significant improvements to the modelling of the complex North African climate (Tramblay et al. 2013; Romera et al. 2015), where the correct simulation of precipitation is challenging due to the high spatio-temporal variability.

Several studies have already evaluated climate change impacts at high resolution over this area. Most used horizontal grid spacings larger than 20 km (Gao et al. 2006; Driouech et al. 2010), with a few studies going down to under 15 km within the framework of the Coordinated Regional Climate Downscaling Experiment database (CORDEX) (Tramblay et al. 2013; Marchane et al. 2017; Fantini et al. 2018; Tramblay et al. 2018). However, these studies usually focus on the Mediterranean as a whole, or on Morocco or the Iberian Peninsula separately. Overall, they have confirmed the trends exhibited by the GCMs, highlighting the region's particular vulnerability to climate change. For instance, Tramblay et al. (2013) predicted a reduction in precipitation of up to 19% and a temperature rise of 1.9 °C by mid-century over the Makhazine catchment in northern Morocco.

Still, past studies have a number of limitations. First, the choice of the forcing GCM is, to the best of our knowledge,

not discussed, whereas it is well-known that various GCMs have different biases and some are not able to correctly model the climate in given regions (Tebaldi et al. 2005; McSweeney et al. 2015). Bias correction is the preferred option to tackle this problem, but some GCMs may not be able to accurately represent large-scale climate drivers and known teleconnections, thus diminishing our confidence in their projections. Besides, as noted by Tramblay et al. (2013), bias correction for precipitation yields unsatisfactory results even in 12 km-resolution RCMs forced with reanalysis data. Second, and most important, the physical mechanisms behind projected regional climate changes are not discussed. Because the Southwestern Mediterranean exhibits such robust drying trends, it is important to put the RCM results in the context of regional and global trends simulated by the coarse-resolution GCM. An important question is to determine to what extent the physical mechanisms behind the drying at the finer RCM scale are consistent with those identified in GCMs (Tuel and Eltahir 2020), and whether they are better represented at higher resolution.

The goal of this study is to conduct high-resolution (12 km) regional climate simulations over the Southwestern Mediterranean to improve the understanding of climate

change processes in this region, with a specific focus on the strong wintertime drying. We apply the MIT Regional Climate Model (MRCM, Im et al. 2014) over a region centered over the Gibraltar Strait and extending from southern Morocco to northern Spain (Fig. 1a). The ability of M RCM to correctly simulate the current regional climate is demonstrated by using boundary conditions guided by observations (ERA-Interim reanalysis, Dee et al. 2011). We then downscale projections from three GCMs from the CMIP5 archive (Taylor et al. 2012) under the historical (1976–2005), RCP4.5 and RCP8.5 (2071–2100) scenarios (Van Vuuren et al. 2011). The GCMs are selected based on their ability to represent the main large-scale features of wintertime climate in the region. Future projections are then analyzed to understand the physical processes responsible for the robust regional precipitation decline and to connect them to larger-scale climate trends in the Mediterranean.

2 Area of study

Our simulation domain, centered at 34°N, 5°W, covers most of Morocco, Portugal and southern Spain (Fig. 1a); we refer to it hereafter as Northwest Africa and Iberian Peninsula (NWAIP). It has 166×161 grid cells with a horizontal resolution of 12 km, sufficient to resolve much of the complex regional topography. Most of the precipitation occurs over Portugal, western Spain and northwestern Morocco, coastal regions which stand under the influence of North Atlantic storm systems (Hurrell et al. 2003, Knippertz et al. 2003). There, the climate is of the Mediterranean type: winters are mild and wet, and summers hot and dry. In Morocco, the Atlas Range acts as a barrier which slows down westerlies, forces orographic precipitation, and cuts off the moisture supply for regions to its east. The Spanish sierras similarly create a rain shadow over southeastern Spain, much drier than the regions to its west. Still, long periods of drought, at any point during the year, and seasonal lack of moisture are common across the domain. Average annual precipitation ranges from 100 mm south of the Atlas, up to about 800 mm over southern Portugal and Morocco's Rif Mountains. The vast majority of it falls during the wet season, from November to May. Storm events during this period are few, short and irregular (Born et al. 2008), occurring as mid-latitude weather systems drifting south-eastward from the North Atlantic. Their frequency increases with latitude, as one gets closer to the storm track center. A large fraction of the winter precipitation falls as snow over the Atlas Range and Iberian sierras, building up a snowpack which slowly melts over spring, guaranteeing a prolonged water supply for the plains below. South and southeast of the Atlas, the Sahara Desert is characterized by a year-round hot and dry climate with less than 100 mm of rain.

Coupled to this spatial variability, rainfall is also highly variable in time, with an inter-annual coefficient of variation ranging from 25% along the Atlantic coast up to 100% in the most arid regions. The main driver of inter-annual winter precipitation variability in the NWAIP is the North Atlantic Oscillation (NAO), an oscillatory pattern of sea-level pressure between the Azores High to the south and the Icelandic Low to the north (Hurrell et al. 2003). High values of the NAO are associated with a northwards-displaced storm track and dry conditions south of 40°N; negative values, on the other hand, lead to wetter-than-average conditions over southern Spain, Portugal and Morocco.

For a detailed characterization of rainfall and temperature changes across this complex region, we divide the land area in our domain into several sub-regions. Relevant to precipitation projections, we select five major watersheds: the Tajo and Guadalquivir, in southern Spain and Portugal, and the Loukkos, Sebou and Oum-Er-Rbia watersheds in Morocco (Fig. 1b). The last three provide about 70% of river discharge in Morocco (MEMEE 2009) and their water resources are therefore critical for the country. We analyze both winter (DJF) and spring (MAM) seasons, since each accounts for 30–40% of annual rainfall over most of the NWAIP domain. For temperature projections, we focus on coastal and mountainous (above 1200 m) regions in winter (DJF) and summer (JJA). Specifically, we consider the Atlas Range in Morocco and the Sierra Nevada in southern Spain, two areas characterized by an important winter snowpack and therefore highly vulnerable to warming (Fig. 1c).

3 Model description and experimental design

3.1 The MIT regional climate model (MRCM)

MRCM (Im et al. 2014) is based on the ICTP-Regional Climate Model Version 3 (RegCM3, Pal et al. 2007). MRCM maintains much of the same structure but incorporates several significant enhancements, including coupling of the Integrated Biosphere Simulator (IBIS) land surface scheme (Winter et al. 2009), a new surface albedo assignment (Marcella and Eltahir 2012), modified boundary layer height and boundary layer cloud schemes (Gianotti 2012), an irrigation scheme (Marcella and Eltahir 2014), an improved convective cloud scheme (Gianotti and Eltahir 2014a) and a convective rainfall auto-conversion scheme (Gianotti and Eltahir 2014b). With its incorporation of new physical schemes or modification of original schemes, MRCM has consistently showed comparable or better performance in simulating key climate features across various regions (e.g., North America, West Africa, Southwest Asia, and the Maritime Continent) compared to various regional climate models. In particular,

Im et al. (2014) demonstrated from simulations over West Africa that the use of IBIS as the land surface scheme results in better representation of surface energy and water budgets in comparison to RegCM3′s BATS. Additionally, Pal and Eltahir (2016) improved the skill of MRCM in simulating the key surface processes over the desert of southwest Asia, thanks to a new albedo prescription based on NASA/GEWEX Surface Radiation Budget (SRB) project and emissivity from NASA MODIS surface emissivity data.

In consideration of the good performances from these previous studies, we adopt the same combination of physical parameters and land surface conditions as in Pal and Eltahir (2016) except for the convection scheme, for which we select the Grell scheme with Fritsch-Chappell closure assumption. This choice is based on results of test simulations among all possible schemes (Emanuel or Grell scheme with either Arakawa/Schubert or Fritsch/Chappell cumulus closure scheme) to select the one that simulates observations best. We run the model at a resolution of 12 km. The following physical schemes are employed in our experiment: the IBIS land surface scheme; the sub-grid explicit (SUBEX) moisture scheme (Pal et al. 2000); the radiation package of the National Center for Atmospheric Research (NCAR) Community Climate Model, version 3 (CCM3) (Kiehl et al. 1996); the nonlocal planetary boundary layer scheme (Holtslag et al. 1990); and the ocean–atmosphere flux algorithm proposed by Zeng et al. (1998).

3.2 Experiment design

First, we evaluate the model's performance in simulating key processes of the regional climate by performing a dynamical downscaling of the ERA-Interim reanalysis dataset (Dee et al. 2011) with MRCM over the 30-year 1981–2011 period. In this experiment, MRCM is driven by the $1.5° \times 1.5°$ 6-h ERA-Interim data as lateral boundary conditions and the $1° \times 1°$ weekly National Oceanic and Atmospheric Administration (NOAA) optimum interpolation sea surface temperatures (OISST, Reynolds et al. 2002) over oceans. We

select the optimal convection scheme in this setting. This simulation is afterwards referred to as ERA/MRCM.

Spatial patterns and regional means of temperature and precipitation are compared to several datasets for robustness, given that no single dataset may perform best over our whole area: first, to TerraClimate (Abatzoglou et al. 2018), which is based on station and reanalysis data, and is available from 1950 to present at a 4 km resolution. Second, to the Tropical Rainfall Measuring Mission (TRMM, Huffman et al. 2007) 3B43 version 7 precipitation dataset, which is based on remotely-sensed data corrected with station observations at the monthly timescale, available from 1998 to present at a 0.25° resolution. Third, to the Iberia01 dataset (Herrera et al. 2019), which covers the 1971–2015 period at a 0.1° resolution and is based on a high density of stations covering the Iberian Peninsula. TRMM has been found to perform well over Morocco, where the station network is sparse (Milewski et al. 2015); TerraClimate has been validated in the Mediterranean, but against Global Historical Climatology network stations only (Abatzoglou et al. 2019).

Second, we perform climate change experiments using the same configuration of MRCM as in ERA/MRCM, but with 6-h output from three selected GCMs from the CMIP5 data archives ("r1i1p1" ensemble members) used as lateral boundary conditions. The selection process is described in Sect. 3.3. The 1975–2005 period forced by historical GHG concentrations is taken as reference, and compared with the 2070–2100 period forced by the Representative Concentration Pathways (RCP) 4.5 and RCP8.5 emission scenarios (Van Vuuren et al. 2011). In total, nine 31-year GCM runs are dynamically downscaled with MRCM.

In all simulations, the first year is discarded as spin-up, leaving 30-year projections (1976–2005 for reference, 2071–2100 for future and 1982–2011 for ERA/MRCM) to be analyzed. We also statistically correct the mean biases of surface temperature and precipitation from MRCM simulations at the monthly time-scale with a parametric quantile mapping technique (Sect. 3.4). A summary of the ten MRCM runs is given in Table 1.

Table 1 Summary of the ten MRCM simulations

	Boundary conditions	Scenario	Simulation period
Reanalysis downscaling	ERA-Interim + OISST	N/A	1982–2011
Climate change simulations	MPI-ESM-MR	Historical	1976–2005
		RCP4.5	2071–2100
		RCP8.5	2071–2100
	GFDL-ESM2M	Historical	1976–2005
		RCP4.5	2071–2100
		RCP8.5	2071–2100
	IPSL-CM5A-LR	Historical	1976–2005
		RCP4.5	2071–2100
		RCP8.5	2071–2100

3.3 GCM selection

We select suitable GCMs to use as forcing boundary conditions for MRCM. GCMs are selected among all CMIP5 participating models for which 6-h data is available, according to the following methodology:

1. First, given the dominant role played by the NAO in driving inter-annual precipitation variability over our domain, we first retain thirteen models that are able to capture some of the main features of the NAO, based on the comprehensive analyses by Davini and Cagnazzo (2014) and Wang et al. (2017), and for which 6-h output data is available. The model list is given in Table S1.

2. Second, we exclude the GCMs that are unable to simulate the impact of the NAO on southwestern Mediterranean precipitation (15°W–0°/30–40°N) during winter. This impact is quantified by the correlation of the DJF NAO index and concurrent precipitation (Fig. 2). Two procedures are tested to compute the NAO index in GCMs: first, as the time series of the first principal component of DJF sea-level pressure (SLP) over the North Atlantic (90°W–40°E and 20–80°N), and second, as the projection of annual DJF SLP fields onto the «observed» NAO pattern, defined as the first principal component of

DJF SLP in the NCEP-NCAR reanalysis (Kalnay et al. 1996) (Fig. 2a–d). Both approaches yield similar results, though each has its limitations, as discussed in Davini and Cagnazzo (2014). We also assess the ability of GCMs to reproduce the spatial patterns of DJF SLP correlation to Western Mediterranean precipitation, based on spatial correlation coefficients (Fig. 2e–h). Table S2 summarizes the performance of the 13 GCMs selected in step 1.

3. Finally, the historical simulations from the selected GCMs are evaluated over the domain, by looking at climate variables during winter and spring relevant for the present analysis: temperature, relative humidity and precipitation. Spatial patterns and regional means are compared to the datasets discussed in Sect. 3.2.

We select three GCMs at the end of this screening process: GFDL-ESM2M (Dunne et al. 2012), IPSL-CM5A-LR (Dufresne et al. 2013) and MPI-ESM-MR (Giorgetta et al. 2013). These three GCMs generally show the best or close to best performance for the criteria introduced in step 2 (Table S2). Although they all suffer from an evident dry bias (common in fact to most, if not all, CMIP5 GCMs, partly connected to the poor representation of the regional orography, which plays an important role in forcing winter
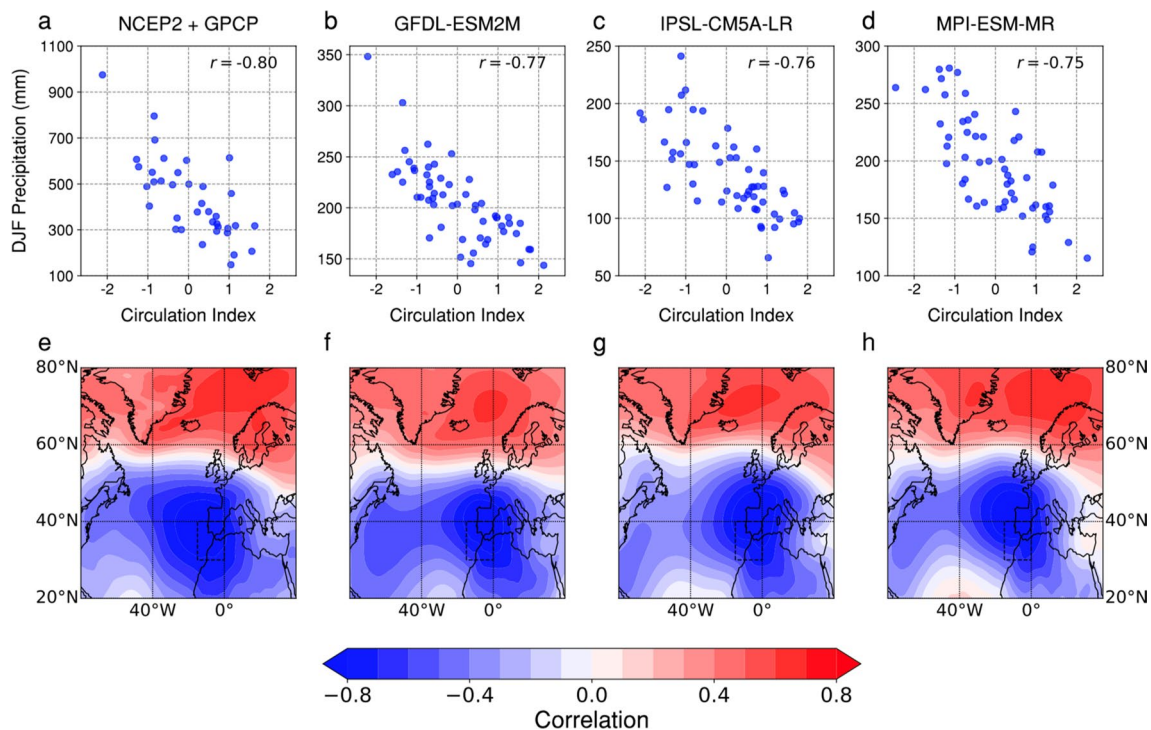

Fig. 2 a–d DJF Western Mediterranean (15°W–0°/30–40°N) precipitation against concurrent NAO circulation index (see text for definition), with correlation coefficients indicated at top-right; and (**e–h**) Pearson correlation of DJF SLP to concurrent Western Medi-

terranean precipitation, in (**a**, **e**) GPCP and NCEP-NCAR reanalysis (1979–2017); (**b**, **f**) GFDL-ESM2M; (**c–g**) IPSL-CM5A-LR; and (**d**, **h**) MPI-ESM-MR. For (**b–h**) data covers the 1950–2004 period

precipitation), they accurately reproduce the SLP-precipitation relationship during winter.

3.4 Bias correction

Output from regional climate modelling experiments contains systematic biases arising, among others, from lateral boundary conditions and imperfect representation of physical processes (Liang et al. 2008; Ehret et al. 2012). To reduce this bias, we apply a parametric quantile mapping (QM) method based on cumulative distribution functions (CDF) to monthly-mean temperature and precipitation at each grid point in the domain (Li et al. 2010). Normal (gaussian) and gamma distributions are commonly used for representing the probability density function of temperature and precipitation, respectively. We fit here normal distributions to monthly mean temperatures and gamma distributions to monthly-mean precipitation in both observations and model output, at each grid point and separately for each month. Then, the parametric QM technique consists in correcting the model CDF to match the observed one. As usual in bias correction methods, this transformation is assumed to be remain valid for future climate projections, so the same bias correction is also applied to future temperature

and precipitation. For observation datasets, we use for both temperature and precipitation TerraClimate (Abatzoglou et al. 2018), one of the best available consistent long-term and fine-scale gridded observational records. Since Terra-Climate (~ 4 km) and MRCM (12 km) have different grid size, TerraClimate is first regridded to the 12 km MRCM grid resolution.

4 Results

4.1 MRCM performance

We first assess the performance of ERA/MRCM by comparing the simulated precipitation to TRMM, Iberia01 and TerraClimate data, focusing on the climatology over our domain and inter-annual variability for the winter season. While the GCM ensemble mean (ENS/GCM) is able to broadly capture the overall precipitation gradient between the wetter regions over the Iberian Peninsula and the dry desert over northwest Africa, the small-scale maxima along the African coastlines and over the high mountainous regions are, unsurprisingly, missed (Fig. 3). Figure 3c makes clear the overall dry bias of GCMs over Morocco, expected since high-altitude regions
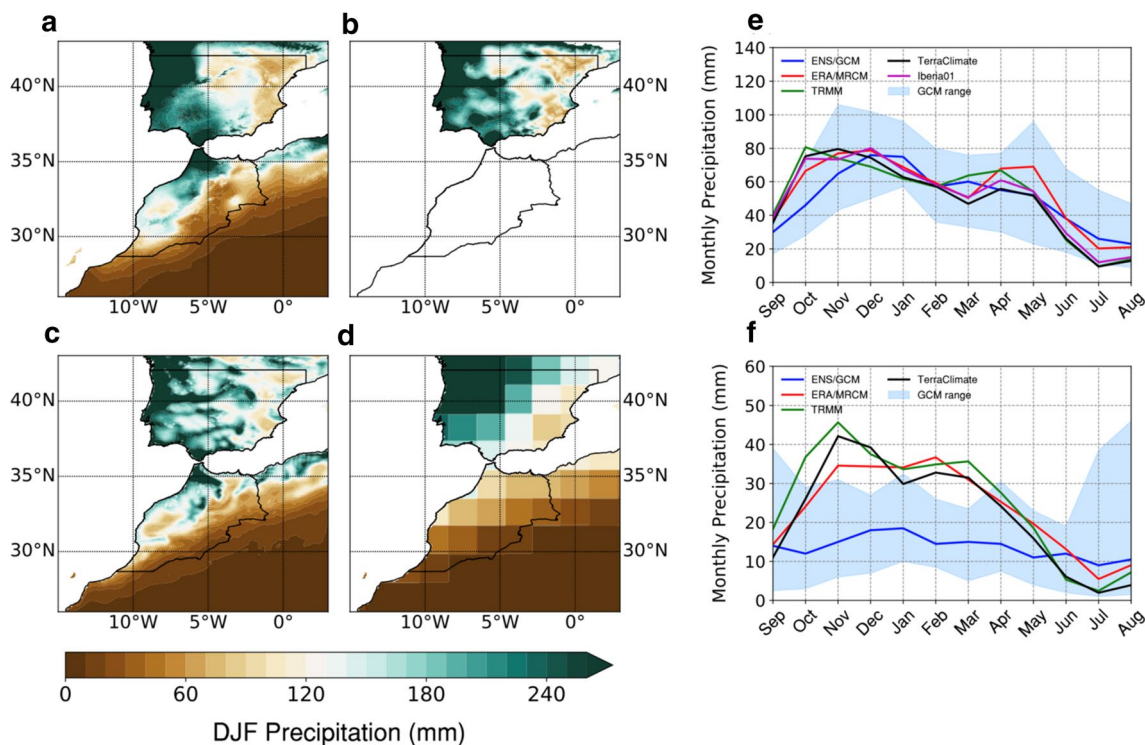

Fig. 3 **a–d** Spatial distribution of 30-year climatology of average DJF total precipitation over the NWAIP: **a** TerraClimate, **b** Iberia01, **c** MRCM-downscaled ERA-Interim (ERA/MRCM), **d** ensemble mean of 13 CMIP5 GCMs (ENS/GCM) (see Table S1). **e–f** Annual cycles of monthly land precipitation averaged over **e** the southern Iberian Peninsula and **f** northwestern Morocco [see black contours in (**a–d**)], in TerraClimate (black), Iberia01 (magenta, **e** only), TRMM (green), ERA/MRCM (red) and ENS/GCM (blue). The light blue shading corresponds to inter-GCM spread in the 13-member GCM ensemble

that receive the most precipitation are not resolved at all (Fig. S1). In contrast, ERA/MRCM is in good agreement with the distribution in TerraClimate and Iberia01, both at large- and small-scales. DJF precipitation over the Moroccan and Algerian coastlines is overestimated, as is the case in central Spain, although there TerraClimate exhibits a noticeable dry bias compared to Iberia01, which agrees very well with ERA/MRCM (Fig. 3b, c). The density of stations used to obtain the data being much higher. South of the Atlas Range, precipitation is also slightly overestimated, possibly a consequence of the incorrect representation of summer small-scale convective systems which bring a large fraction of annual precipitation in this region. Still, MRCM exhibits a pronounced precipitation downscaling skill, especially in regions where orographic forcing dominates. As to annual cycles (Fig. 3d, e), the ENS/GCM is quite able to capture the seasonal variation of precipitation over the Iberian Peninsula, with its maximum in winter and minimum in summer. The magnitude of wet-season precipitation is reasonably close to TerraClimate, with an evident dry bias all the same.

Summer precipitation is quite overestimated, however. By contrast, over northwestern Morocco, GCMs fail to capture the seasonal cycle, showing instead a somewhat constant monthly precipitation rate. The dry bias during winter and spring is evident. Additionally, inter-GCM spread is quite large, especially between July and September when some GCMs produce copious amounts of precipitation, probably the result of exaggerated tropical moisture transports typically responsible for much of the summer precipitation south of the Atlas Range (Born et al. 2008). Compared to ENS/GCM, ERA/MRCM is in good agreement with TerraClimate, especially over northwestern Morocco, though it fails to fully capture the bimodal distribution with two peaks in December and March as evident in TerraClimate. GCM biases over the Iberian Peninsula, especially a peak in precipitation around May and the underestimation of late fall precipitation, are not fully corrected.

As to inter-annual variability, it is remarkably well captured by ERA/MRCM. Figure 4 shows the time series of DJF precipitation anomalies (defined with respect to
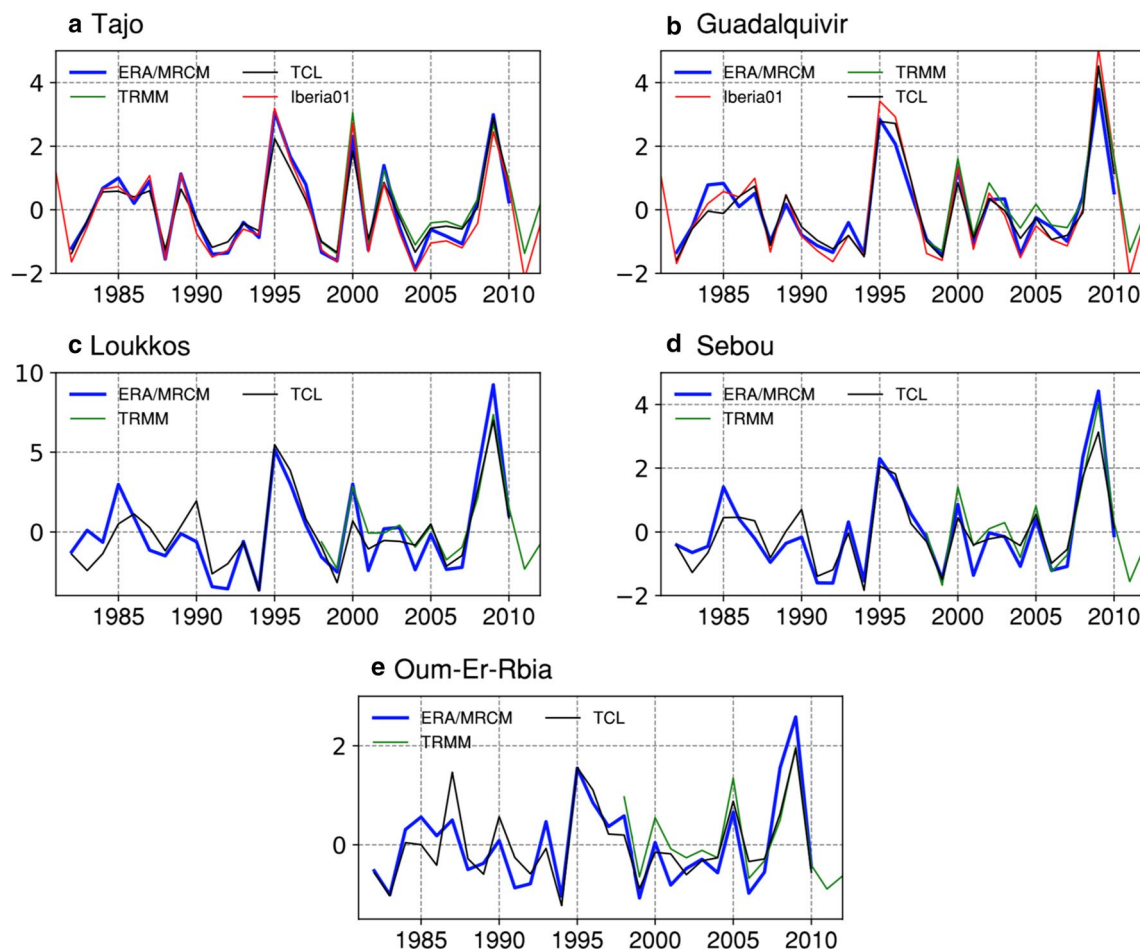

Fig. 4 Annual DJF precipitation anomalies averaged over the five selected watersheds, in TerraClimate (TCL, black), Iberia01 (red, in **a**, **b**), TRMM (green) and ERA/MRCM (blue). Anomalies, in mm/day, are defined by subtracting to each series its 1982–2011 average

each series' 1982–2011 mean), over the five selected watersheds (Fig. 1b). Anomaly correlation coefficients range from 0.91 to 0.98, which shows that MRCM, for this domain and at the 12 km resolution, is able to correctly simulate the precipitation response to large-scale, NAO-linked storm track shifts present in the boundary conditions.

In summary, ERA/MRCM shows satisfactory performance in simulating both the average and the inter-annual variability of winter precipitation over the NWAIP domain. Even though GCM biases translate to the downscaled simulations, the improved representation of topography helps

to compensate in part for GCM's dry bias during the wet season.

4.2 Verification of bias corrected MRCM runs

Before analyzing future projections, we validate the performance of the bias corrected GCM-driven MRCM runs (ENS_BC/MRCM) for the reference period, by comparing their results with those from ERA/MRCM and TerraClimate observations. Figures 5 and 6 show the spatial distribution of the 30-year monthly precipitation and surface mean temperature climatologies for the winter season (DJF) derived
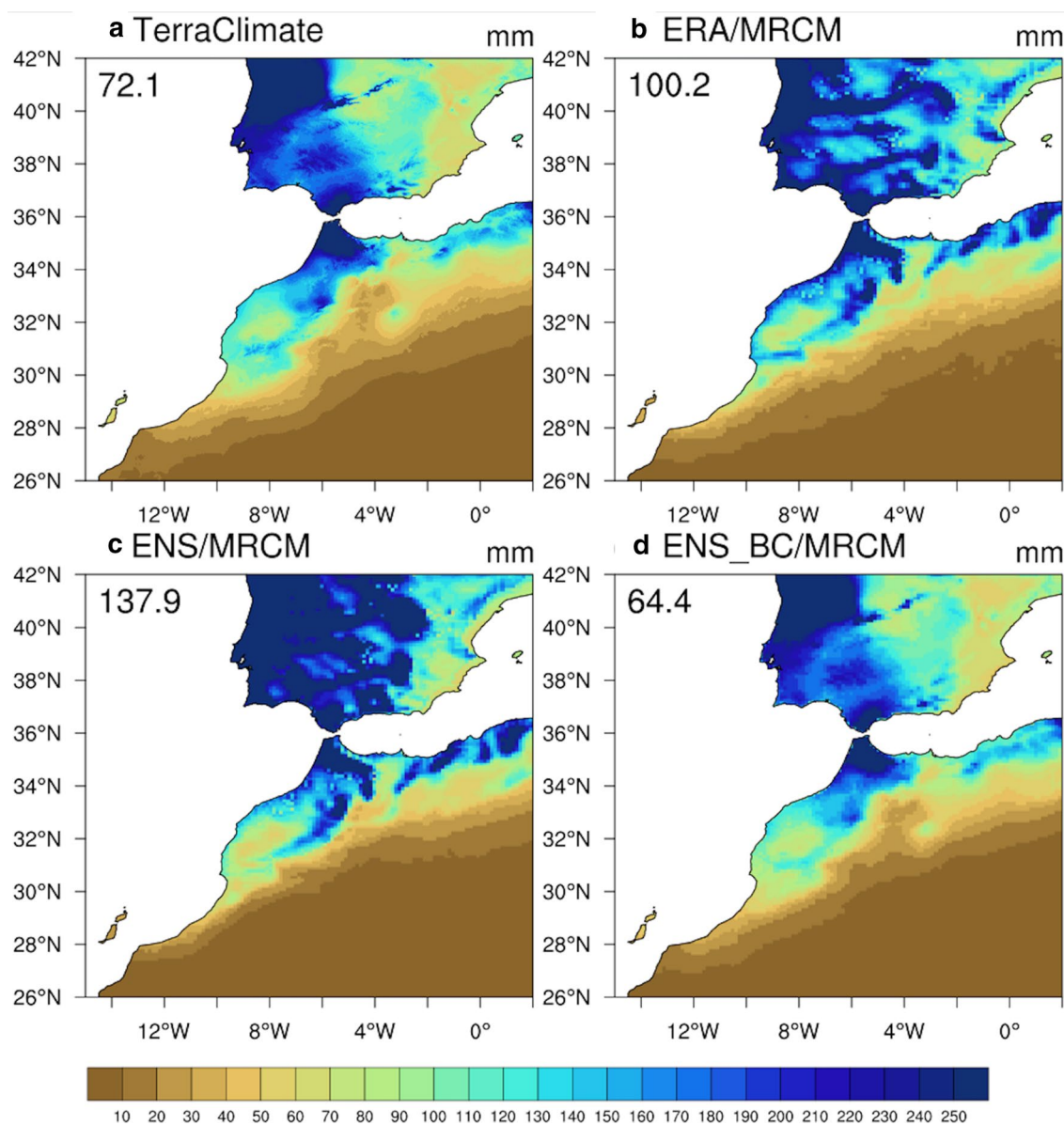

Fig. 5 Spatial distribution of 30-year climatology of DJF average land precipitation in **a** TerraClimate, **b** ERA/MRCM, **c** ENS/MRCM (ensemble mean of MRCM simulations) and **d** ENS_BC/MRCM (ensemble mean of bias-corrected MRCM simulations). Domain-averaged values are indicated at the top left-hand corner of each plot
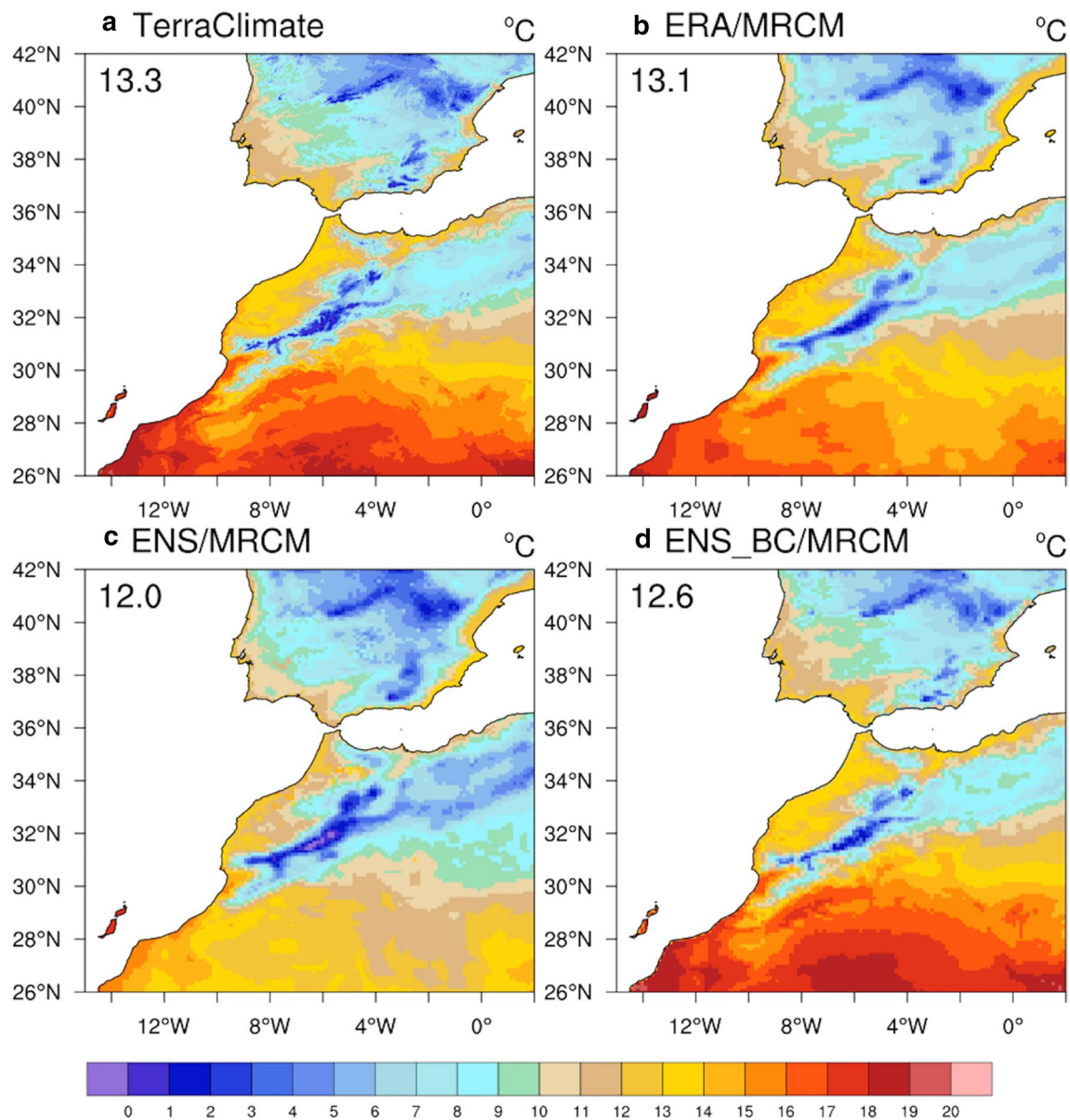
Fig. 6 Same as Fig. 5, for surface temperature

from TerraClimate, ERA/MRCM, ensemble mean of three MRCMs (ENS/MRCM) and ensemble mean of three bias-corrected MRCMs (ENS_BC/MRCM).

For precipitation, ENS/MRCM shows good qualitative correspondence with the observed regional distribution (Fig. 5). However, GCM-driven MRCM runs tend to produce excessive precipitation over higher mountainous regions, particularly over south-central Spain, similarly to the ERA/MRCM run. Wet biases over mountainous areas are indeed a common deficiency in dynamical downscaling, as noted also in other studies (Solman et al. 2008; Gianotti et al. 2012). The exception is IPSL-CM5A-LR, for which the dry bias evident in GCM output (Fig. 2c) is not fully

compensated by the dynamical downscaling. Although it somewhat accurately reproduces long-term NAO dynamics and its relationship to Northern Hemisphere climate variability (Wang et al. 2017), IPSL-CM5A-LR suffers from an "anticyclonic" bias, with a too strong North Atlantic subtropical high that blocks cyclonic activity and leads to the observed dry bias. Regional downscaling cannot compensate for this deficiency.

By comparison with ERA/MRCM and ENS/MRCM, ENS_BC/MRCM is, as expected, in better agreement with TerraClimate in terms of the spatial pattern and area-averaged precipitation. Bias-corrected precipitation is still somewhat lower than observations over the High- and Anti-Atlas

(around 8°W/31°N). Due to the sharp topographic gradients and the scarcity of station data, however, TerraClimate data is undoubtedly less robust in this region.

Regarding mean surface temperatures, the essential characteristics of the mean DJF pattern are accurately reproduced in both ERA/MRCM and ENS/MRCM, since temperatures are strongly constrained by the regional topography. After bias correction, we find that ENS_BC/MRCM successfully captures the observed major characteristics in terms of regional variations and area-averaged values (Fig. 6).

4.3 Future projections

We now focus on future projections of temperature and precipitation over the domain. The bias-correction factors derived from the historical simulation are applied to future monthly-mean temperatures and precipitation in the RCP runs. Future changes are calculated as the difference between

the historical ("Historical") and future simulations (referred to as "RCP4.5" and "RCP8.5").

4.3.1 Precipitation

The spatial distributions of DJF and MAM relative precipitation change under RCP4.5 and RCP8.5 are shown on Fig. 7. A pronounced and robust large-scale precipitation decline over the domain is evident under both scenarios and in both seasons, consistent with the CMIP5 multi-model mean (Tuel and Eltahir 2020) and earlier CMIP5 projections (Giorgi and Lionello 2008). In relative terms, the decline in precipitation is generally larger during spring, at which time the drying is also more extensive, especially over the Iberian Peninsula. While winter precipitation trends in central and Eastern Spain are neither robust nor significant, the situation in spring is quite different. Under RCP8.5, the drying is about twice as large everywhere compared to RCP4.5: from
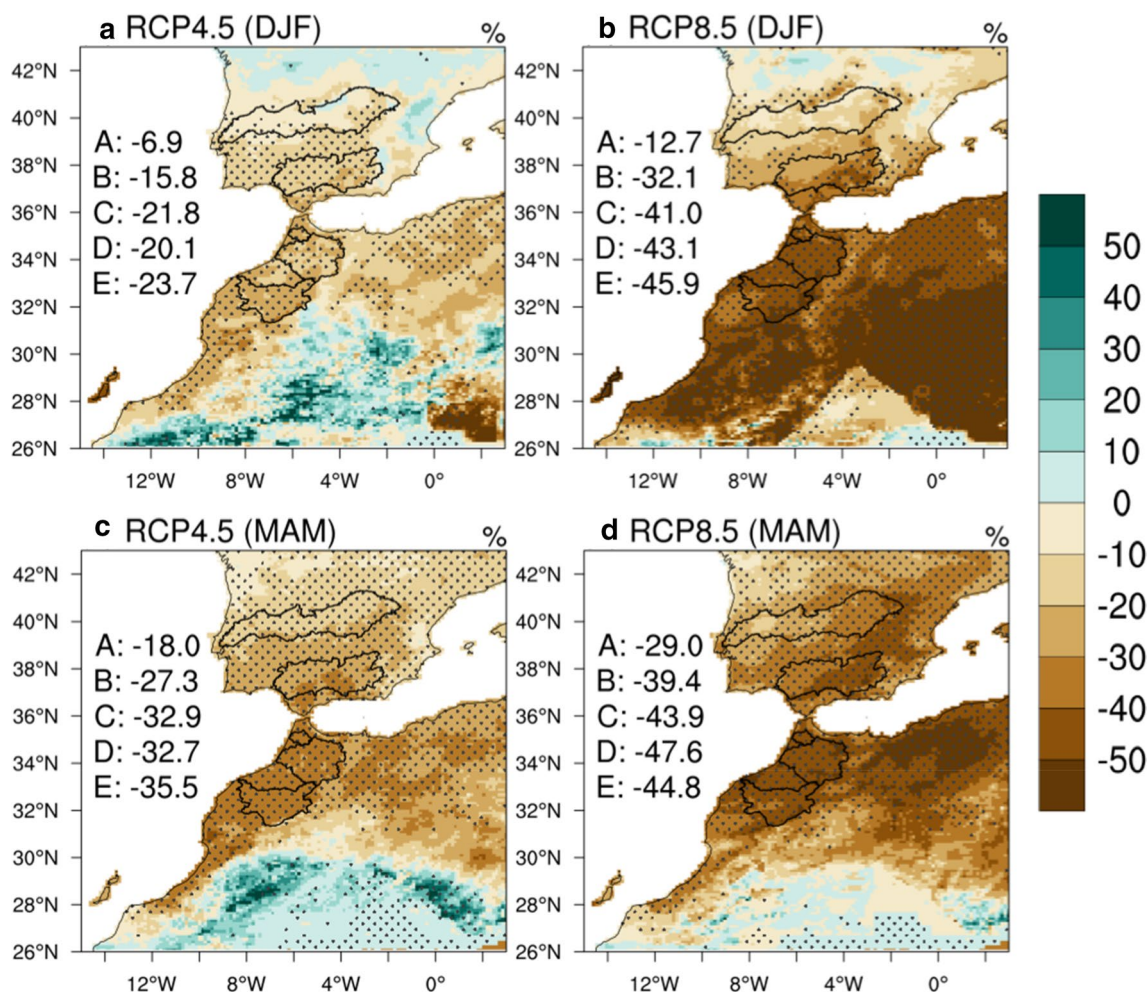

Fig. 7 MRCM ensemble-mean percentage change in **a**, **b** DJF and **c**, **d** MAM precipitation, under **a**, **c** RCP4.5 and **b**, **d** RCP8.5. Mean values averaged over the five watersheds on Fig. 1b are shown on the left-hand side of each plot. Dots indicate agreement by three MRCM simulations on the sign of the change

7–24% to 13–46% (Fig. 7). In MAM, however, the difference between scenarios is smaller: the decrease in precipitation is very strong even with mitigation (RCP4.5). For the region as a whole, the drying gradually weakens from southeast to northwest. In winter, regions north of 40°N even show slight wetting trends, albeit not robust at all. The African coastline is projected to experience the largest drying by far (− 40/45% under RCP8.5), and quite uniformly too: the three Moroccan watersheds show very similar changes in all cases (seasons/scenarios). The southern coast of the Iberian Peninsula is in an intermediate state, with a robust though weaker winter drying.

4.3.2 Temperature

Regarding temperature changes, mean surface temperature is unsurprisingly projected to increase over the whole domain under both RCP scenarios, roughly proportionally

to the radiative forcing (Fig. 8). Similar to the precipitation change, the warming exhibits a pronounced meridional gradient during winter. Temperatures are projected to increase more over North Africa (by 0.5–1 °C), a possible consequence of its more pronounced precipitation decline through decreased latent heating, although dynamical trends may also play a role (see Sect. 5). In winter also, warming trends appear larger over the mountains, especially the High and Middle Atlas, and the Sierra Nevada (Fig. 8a, b). This enhanced warming may be connected to the snow-albedo feedback (Rangwala and Miller 2012; Pepin et al. 2015), since these areas all possess extensive snowpacks in the current climate), although this process is not very well resolved at our 12 km scale and deserves a more detailed treatment (Walton et al. 2017). Rather, since mountain regions receive higher precipitation amounts during winter, they will experience larger absolute drops
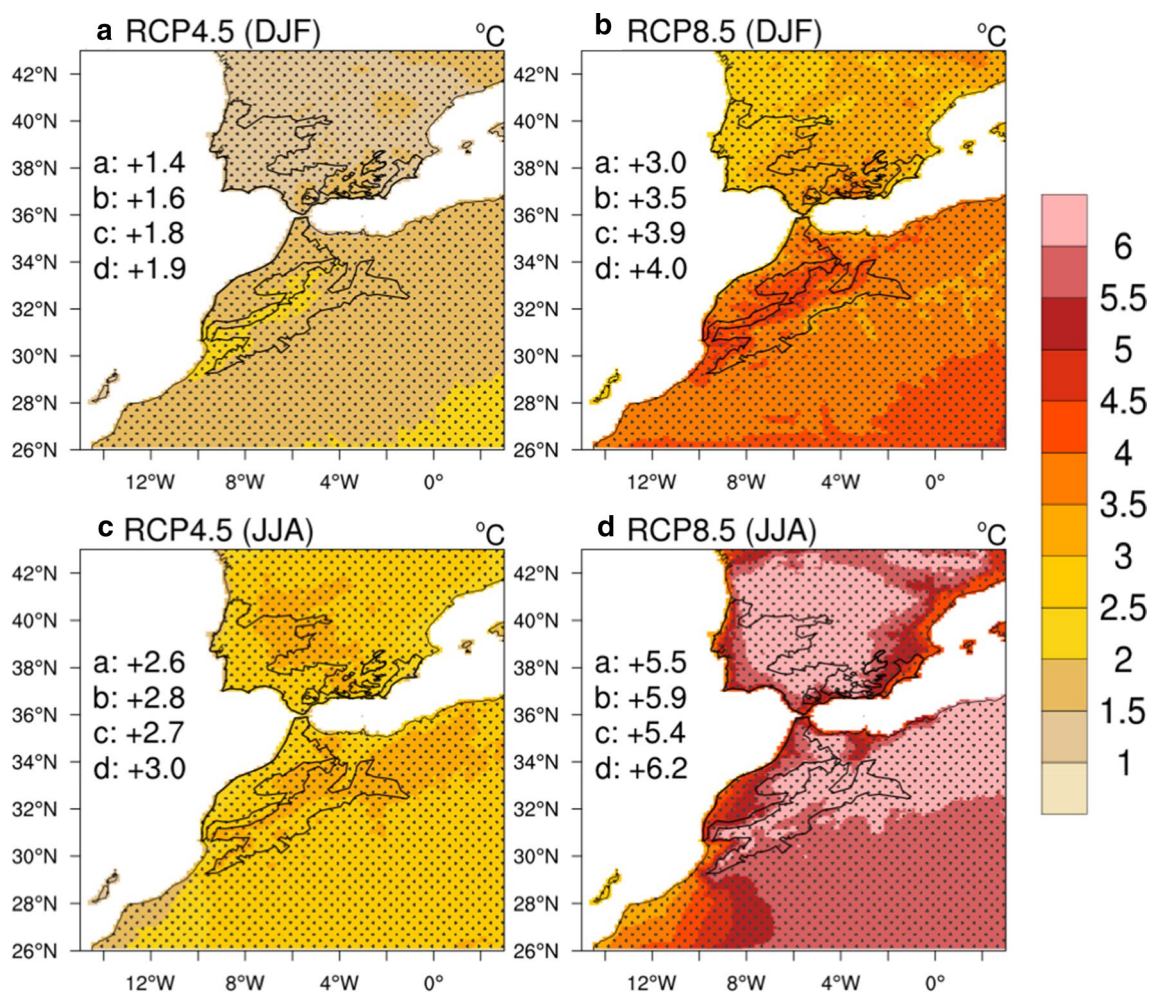

Fig. 8 MRCM ensemble-mean change in **a**, **b** DJF and **c**, **d** JJA surface temperature, under **a**, **c** RCP4.5 and **b**, **d** RCP8.5. Mean values averaged over the four regions on Fig. 1c are shown on the left-hand side of each plot. Dots indicate agreement by three MRCM simulations on the sign of the change

in precipitation, and therefore larger reductions in latent heat flux which will impact on the temperature signal.

In both scenarios, and for all coastal and mountain regions, summer temperature changes are much higher than in winter (by 1–2 °C). They are characterized by a clear coastline/interior contrast, common to all seasons and scenarios, although here again mountain regions seem to exhibit enhanced warming compared to plains, especially the Atlas and the Pyrenees. As in winter, this may be connected to a reduction in precipitation, here brought by summer convective cells quite common at high elevations in this region (Born et al. 2008). The reduced warming along the coasts is a classic feature of climate change linked to less pronounced warming of surface air over oceans.

4.3.3 Mechanisms of precipitation change

We now analyze the physical mechanisms responsible for the robust cold-season drying projected for the region in future simulations. Because the Western Mediterranean is characterized by a steep northeast-southwest humidity gradient, between the relatively moist western side of the Atlas Range, which stands under oceanic influence, and the dry Sahara Desert to the east (Fig. 9a), changes in average winds, however small, can significantly impact the regional moisture distribution. Looking at the MRCM projections under RCP8.5, we find definite trends towards a more easterly kind of circulation in both winter and spring, consistent with the regional picture just mentioned (Fig. 9b). Average changes in just three models are remarkably similar to the much larger CMIP5 multi-model mean (Tuel and Eltahir 2020), underlining the robustness of regional wind trends under continued anthropogenic forcing. Wind changes over North Africa and southern Spain average about 2 m/s at 850 hPa; this must be compared to average westerlies of 1–5 m/s, which is quite weak, even during the wet season when moisture advection from the North Atlantic is largest (Fig. 9a). Storms that hit Morocco and the southern parts of the Iberian Peninsula indeed remain quite rare, even under negative NAO conditions.

The robust shift towards enhanced easterlies, which should lead to enhanced advection of dry air, is consistent with regional projections of atmospheric moisture (Fig. 9b). The northwest African and southern Iberian coastlines stand under relative lows of atmospheric humidity increase, when the rest of the region, particularly northern Spain and Portugal, exhibit much larger wetting trends. The lowest increase is found over the western foothills of the High Atlas. Two factors probably combine to further limit the increase in humidity over this small region. First, the humidity gradient is particularly steep, with the Atlas acting like a barrier between the very dry Sahara and their much moister western flanks. Second, a future circulation with more frequent easterlies will result in strengthened descent of dry air, its moisture having been "squeezed" out as it passed over the mountains. In other words, this region will become a rain shadow as the prevailing winds change direction. This interpretation is further buttressed by the enhanced local wetting on the southeastern side of the Atlas (e.g., around 4°W–32°N, Fig. 9b), which clearly points to enhanced removal of atmospheric water on what is currently the leeward side of the mountain range. Results and conclusions for the RCP4.5 scenario are similar, although the magnitude of the trends is smaller, as expected.

Therefore, for the region as a whole, the circulation shift acts to both increase dry advection, and to cut off the moisture supply from the Atlantic, consistent with the argument proposed by Tuel and Eltahir (2020) on the basis of CMIP5 projections. Relative humidity, however, is not only dictated by moisture content but also temperature (Fig. 9d). Regional projections show a stark enhancement of lower-tropospheric warming in the regions downwind of future wind anomalies, i.e., on the northwestern flanks of the Atlas Range and Sierra Nevada (Fig. 9c, S2-c). At the same time, the warming is relatively weaker, by 1–1.5 °C, on the upslope slide, especially the Saharan Atlas. The geography of the warming and wind change patterns, common to both winter and spring, suggests that topography-driven anomalous vertical motion is an important driver. Strengthened easterlies lead to uplift southeast of the mountain ranges (i.e., upwind) and subsidence on their northwestern slopes (i.e., downwind), respectively associated with adiabatic cooling and warming. Changes in vertical motion near the boundary layer top are consistent with this perspective (Fig. S3). In fact, the more realistic topography in MRCM simulations generates stronger subsidence motion and enhanced warming locally (not shown). While temperature gradients across the Atlas Range are negligible in winter, they strengthen over spring as the Sahara Desert warms up fast (Fig. S4); consequently, enhanced easterlies likely also contribute to the substantial warming over northwestern Morocco and the Algerian coastline at that time of year. Other factors, such as the soil moisture feedback or the snow feedback over the high mountain peaks, may also play a role (Stéfanon et al. 2014; Walton et al. 2017).

We further explore the role of the regional circulation in determining hydroclimate trends by defining, as a proxy for the regional circulation, a wind index along the African coastline (see line in Fig. 9b), where future projections show enhanced easterlies. The value of the index is defined as the direction (in degrees) in which the wind blows; for example, a westerly wind will have an index of 0° and a southerly wind an index of +90°. We focus on the November–April period, the wet season for most of our domain. This index strongly determines to the likelihood of precipitation over Northwestern Morocco and the southern Iberian Peninsula (Fig. 10-a), a relationship that,
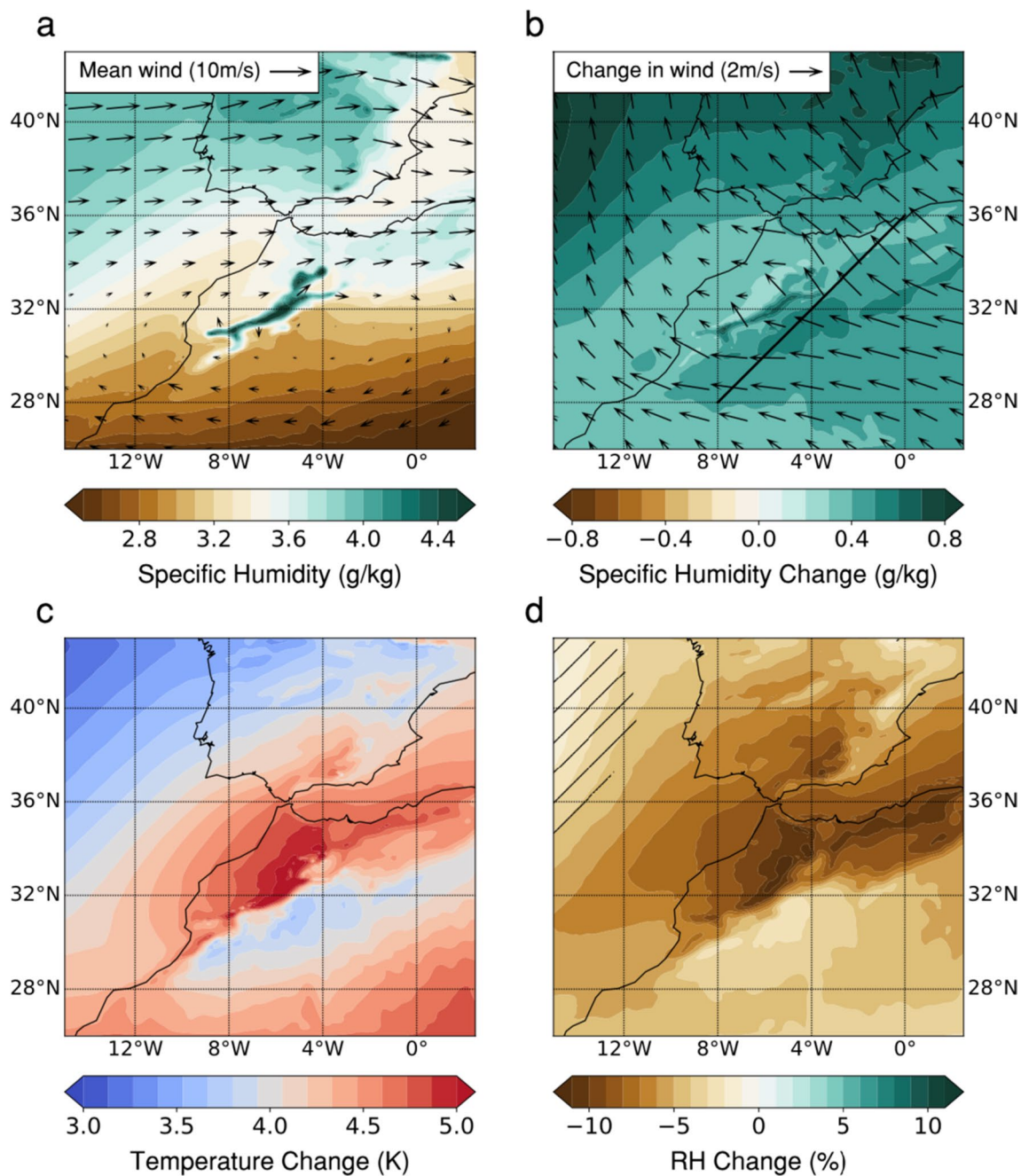
Fig. 9 a DJF MRCM ensemble-mean historical (1976–2011) 850 hPa specific humidity (shaded) and circulation (arrows). **b, c, d** MRCM ensemble-mean change in 850 hPa DJF (**b**) specific humidity (shaded) and circulation (arrows), (**c**) temperature and (**d**) relative humidity. Hatching in **d** indicates disagreement by one of the three models on the sign of the change. The solid black line in **b** is used to define a regional wind index (see main text)

overall, MRCM simulations succeed in capturing (Fig. 10b, S5). Precipitation occurs, as expected, when westerlies prevail (wind index between −45° and 45°). Similarly, easterlies tend to be associated with dry conditions (index higher than 135° or lower than -135°). On the whole, westerlies are more frequent, as would be expected in the midlatitudes during winter. Consistent with regional circulation changes (Fig. 9b), the

frequency of north-westerlies decreases across all simulations (by 10–40% across models), while that of south-easterlies goes up significantly. While westerlies are still the most frequent circulation regime, southeasterly winds (index between 90° and 180°) become much more common. Meteorological conditions during southeasterly days are characterized by a substantial atmospheric moisture deficit over the Iberian Peninsula
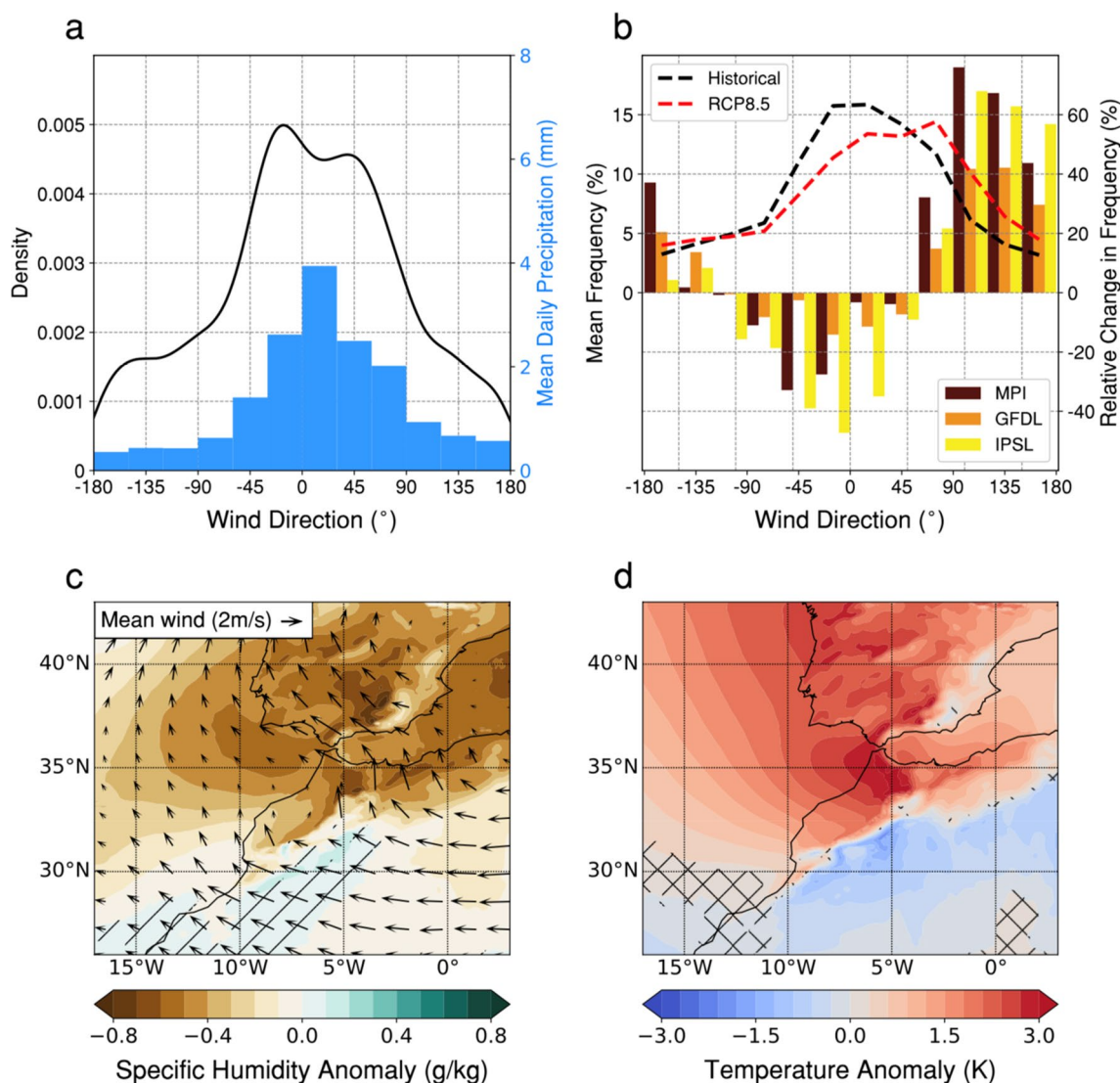
Fig. 10 a Distribution of November–May daily wind index values from ERA-Interim (solid black line) and average daily precipitation from TRMM over northwestern Morocco and the southern Iberian Peninsula (up to 38°N) in each 30-degree wind direction category (blue bars). **b** MRCM ensemble-mean distribution of November–May daily wind index values in the historical (dashed black) and RCP8.5 (dashed red) simulations, and relative change in the frequency of each 30-degree wind index category for the three MRCM runs (colored bars). **c, d** MRCM ensemble-mean average 850 hPa (**c**) specific humidity anomaly (shaded) and wind values (arrows) and **d** temperature anomaly, during "southeasterly days" (when the wind index is between +90° and +180°) in historical simulation. Hatching in **c, d** indicates disagreement by one of the three models on the sign of the anomaly

and along the northwestern African coastline (Fig. 10c), and the wind pattern is very similar to the future projected shift (Fig. 9b). Additionally, southeasterly days exhibit warmer-than-usual temperatures over the same regions with moisture deficit, and cooler-than-usual temperatures on the upwind side of the Atlas and Sierra Nevada, a pattern highly similar to the projected temperature change (Figs. 9c, 10d). This confirms the hypothesis that the circulation shift is responsible for the increase in moisture deficit and enhanced warming seen in regional projections. The combined effects of those mechanisms result in a large decrease in lower-troposphere relative

humidity over Northwestern Morocco and Algeria, southern Spain, and the surrounding ocean (Fig. 9d, S2-c), from which the precipitation decline follows.

5 Discussion

Our downscaling results are consistent with the existing literature which highlighted a pronounced wet-season precipitation decline and enhanced summer warming over the southwestern Mediterranean (Diffenbaugh and Giorgi

2012). These trends are consistent with GCM projections of future Mediterranean winter drying (Seager et al. 2014; Zappa et al. 2015; Tuel and Eltahir 2020) and enhanced summertime warming, though GCM deficiencies may cause the latter to be overestimated (Boberg and Christensen 2012). At the local scale, the detailed representation of the complex regional topography and its spatial variability (Fig. S1), as well as the resolution of convection, lead to improvements in convective and orographic precipitation (Prein et al. 2015), in keeping with the 0.11° experiments from the EURO-CORDEX and Med-CORDEX initiatives (Jacob et al. 2014, Tramblay et al. 2013, Fantini et al. 2018). Our focus in this study was on winter and spring, when convective precipitation remains limited in the region. MRCM showed pronounced downscaling skill for precipitation during these seasons. Summer precipitation, on the other hand, especially in the mountains, remain challenging to simulate, as it is typically associated with small (< 12 km) convective systems that interact with the topography (Born et al. 2008). New perspectives from convection-permitting simulations could help us refine and better understand trends in convective activity in the warm season (Coppola et al. 2020).

Temperature downscaling also allowed us to refine projections for coastal and mountainous regions, that were unresolved in GCMs. For the coast, where most of Morocco's largest cities are located, mean monthly temperatures may reach extremes of 37 °C under the RCP8.5 scenario, a 7 °C increase compared to the present-day distribution. Inland cities currently regularly experience mean temperatures well above that threshold, but the relative humidity is much lower there than on the coast, where it remains high even at the peak of summer. This means that summer days may become significantly more uncomfortable in cities like Rabat or Casablanca. This large temperature increase, even under a mitigation scenario, could have significant impacts on Morocco's economy, notably its tourism and agriculture. Higher temperatures—along with increased dryness—in winter, after sowing, and in spring, during grain filling, would certainly impact cereal yields.

At the regional scale, future projections exhibit dynamical trends characterized by enhanced easterly flow, consistent with basin-wide circulation trends consisting in the development of a strong anticyclone centered on the Mediterranean Basin (Tuel and Eltahir 2020) (Fig. 11). This pronounced anomalous high, highly robust across GCMs, finds its origin in the combination of large-scale shifts in winter planetary waves due to the strengthening of the mid-latitude jet (Simpson et al. 2016), and to the reduced warming of the Mediterranean Sea with respect to the surrounding land, and its magnitude essentially determines that of the regional winter drying (Tuel and Eltahir 2020). In GCMs, the dry advection effect of this anomalous wind dominates in the precipitation trends; regional simulations show, however, how
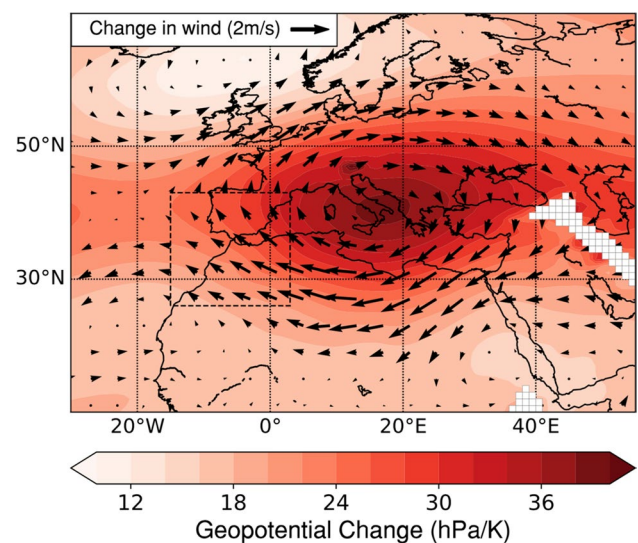

Fig. 11 CMIP5 multi-model change in DJF 850 hPa geopotential height and wind over the Mediterranean, using the 13 GCMs of Table S1. Our domain region is shown by the dashed black line

the anomalous wind also interacts with the topography to enhance the warming and drying pattern (Fig. 9c, d).

This regional drying is probably the most critical feature of the climate response to anthropogenic forcing in the Western Mediterranean. Together with enhanced temperatures, it will drive substantial declines in river runoff and water availability and severely threaten the habitability of the region. We can expect that the future changes in net precipitation (accounting for evaporation) will follow those of precipitation, as suggested by Tramblay et al. (2018), since evaporation in the NWAIP tends to be more constrained by water availability than by incoming energy. Further analysis using either hydrological models or simple runoff coefficient estimates could provide more detailed estimates of the decline in river flow for the region.

6 Summary and conclusion

In this study, we sought to project and understand the future wintertime climate of the southwestern Mediterranean, specifically the intense drying that characterizes this region in global climate projections. We performed high-resolution climate downscaling and projections with MRCM driven by the ERA-Interim reanalysis and three carefully-selected GCMs from the CMIP5 archive that correctly represent large-scale feature of winter climate over the NWAIP region. At our 12 km resolution, MRCM showed reliable downscaling skill as tested against observed station- and satellite-based gridded climate products. Projections under the RCP4.5 and RCP8.5 scenarios show a severe precipitation

decline over much of the region during the wet season, and strong warming during summer, especially in continental interiors. Local changes in temperature and precipitation are consistent with GCM trends but strongly influenced by the complex topography, and can locally be of higher magnitude, as in the case of warming at high elevations. Temperature and precipitation trends are connected to changes in Mediterranean circulation that translate into enhanced easterly flow over the NWAIP, which, by advecting dry Saharan air and by interacting with the regional orography, lead to a pronounced low-level warming and precipitation decline.

The results of this study underline the high vulnerability of the Western Mediterranean to climate change. This vulnerability is due to its geographical location downwind of a large and very dry desert. In addition, the substantial role played by fine-scale topography and its interaction with regional circulation change make a strong case for the use of high-resolution models in the region. While the selection of GCMs for downscaling could be improved upon, the identified physical mechanisms behind the drying appear robust enough to be found in all regional simulations. Their better understanding that follows from our results may help further constrain the spread of Western Mediterranean future projections.

References

Abatzoglou JT, Drobowski SZ, Parks SA, Hegewisch K (2018) Terra-Climate, a high-resolution global dataset of monthly climate and climatic water balance from 1958–2015. Sci Data 5:170191

Balaghi R, Jlibene M, Tychon B, Heerens H (2012) Agrometeorological forecasting of cereal crop yields in Morocco. Morocco, National Institute for Agronomic Research (INRA)

Boberg F, Christensen J (2012) Overestimation of Mediterranean summer temperature projections due to model deficiencies. Nature Clim Change 2:433–436

Born K, Fink AH, Paeth H (2008) Dry and wet periods in the northwestern Maghreb for present day and future climate conditions. Meteorol Z 17(5):533–551

Coppola E et al (2020) A first-of-its-kind multi-model convection permitting ensemble for investigating convective phenomena over Europe and the Mediterranean. Clim Dyn 55:3–34

Davini P, Cagnazzo C (2014) On the misinterpretation of the North Atlantic Oscillation in CMIP5 models. Clim Dyn 43:1497–1511

Dee DP et al (2011) The ERA-Interim reanalysis: configuration and performance of the data assimilation system. Q J Roy Meteorol Soc 137:553–597

Diffenbaugh NS, Giorgi F (2012) Climate change hotspots in the CMIP5 global climate model ensemble. Climatic Change 114:813–822

Driouech F, Déqué M, Sánchez-Gómez E (2010) Weather regimes–Moroccan precipitation link in a regional climate change simulation. Global Planet Change 72:1–10

Dubrovsky M, Hayes M, Duce P, Trnka M, Svoboda M, Zara P (2014) Multi-GCM projections of future drought and climate variability indicators for the Mediterranean region. Reg Environ Change 14:1907–1919

Dufresne J et al (2013) Climate change projections using the IPSL-CM5 Earth System Model: from CMIP3 to CMIP5. Clim Dyn 40:2123–2165

Dunne JP et al (2012) GFDLs ESM2 global coupled climate-carbon earth system models. Part I: physical formulation and baseline simulation characteristics. J Clim 25:6646–6665

Ehret U, Zehe E, Wulfmeyer V, Warrach-Sagi K, Liebert J (2012) Should we apply bias correction to global and regional climate model data? Hydrol Earth Syst Sci Discuss 9:5355–5387

Fantini A et al (2018) Assessment of multiple daily precipitation statistics in ERA-Interim driven Med-CORDEX and EURO-CORDEX experiments against high resolution observations. Clim Dyn 51:877–900

Gao X, Pal JS, Giorgi F (2006) Projected changes in mean and extreme precipitation over the Mediterranean region from a high resolution double nested RCM simulation. Geophys Res Lett 33:L03706

Giorgetta MA et al (2013) Climate and carbon cycle changes from 1850 to 2100 in MPI-ESM simulations for the coupled model intercomparison project phase 5. J Adv Model Earth Syst 5:572–597

Giorgi F, Lionello P (2008) Climate change projections for the Mediterranean region. Global Planet Change 63:90–104

Gianotti RL (2012) Convective cloud and rainfall processes over the Maritime continent: simulation and analysis of the diurnal cycle. Ph.D. dissertation, Massachusetts Institute of Technology, 306

Gianotti RL, Eltahir EAB (2014a) Regional climate modeling over the Maritime Continent. Part I: new parameterization for convective cloud fraction. J Climate 27:1488–1503

Gianotti RL, Eltahir EAB (2014b) Regional climate modeling over the Maritime Continent. Part II: new parameterization for autoconversion of convective rainfall. J Climate 27:1504–1523

Holtslag AAM, De Bruijn EIF, Pan HL (1990) A high resolution air mass transformation model for shortrange weather forecasting. Mon Wea Rev 118:1561–1575

Huffman GJ et al (2007) The TRMM multi-satellite precipitation analysis (TMPA): quasi-global, multiyear, combined-sensor precipitation estimates at fine scales. J Hydrometeorol 8(1):38–55

Hurrell JW, Kushnir Y, Ottersen G, Visbeck M (2013) An Overview of the North Atlantic Oscillation, In: JW Hurrell, Y Kushnir, G Ottersen, M. Visbeck (eds). The North Atlantic Oscillation: climatic Significance and Environmental Impact. https://doi.org/10.1029/134GM01

Im ES, Gianotti RL, Eltahir EAB (2014) Improving the simulation of the West African Monsoon using the MIT Regional Climate Model. J Clim 27:2209–2229

IPCC (2013) Climate change 2013: the physical science basis. Contribution of working group I to the fifth assessment report of the intergovernmental panel on climate change. Cambridge University Press, Cambridge, New York, p 1535

Jacob D et al (2014) EURO-CORDEX: new high-resolution climate change projections for European impact research. Reg Environ Change 14:563–578

Kalnay E et al (1996) The NCEP/NCAR 40-Year reanalysis project. Bull Amer Meteor Soc 77:437–472

Kiehl JT et al. (1996) Description of the NCAR Community Climate Model (CCM3). NCAR Tech. Note NCAR/TN-4201STR, 152 pp. https://doi.org/10.5065/D6FF3Q99

Knippertz P, Christoph M, Speth P (2003) Long-term precipitation variability in Morocco and the link to the large-scale circulation in recent and future climates. Meteorol Atmos Phys 83:67–88

Liang X, Kunkel K, Meehl G, Jones R, Wang J (2008) Regional climate models downscaling analysis of general circulation models present climate biases propagation into future change projections. Geophys Res Lett 35:L08709

Li H, Sheffield J, Wood EF (2010) Bias correction of monthly precipitation and temperature fields from Intergovernmental Panel on

Climate Change AR4 models using equidistant quantile matching. J Geophys Res 115:D10101

Marchane A, Tramblay Y, Hanich L, Ruelland D, Jarlan LD (2017) Climate change impacts on surface water resources in the Rheraya catchment (high-atlas, Morocco). Hydrol Sci J 62(6):979–995

Marcella M, Eltahir EAB (2012) Modeling the summertime climate of Southwest Asia: the role of land surface processes in shaping the climate of semiarid regions. J Climate 25:704–719

Marcella M, Eltahir EAB (2014) Introducing an irrigation scheme to a regional climate model: a case study over West Africa. J Climate 27:5708–5723

McSweeney CF, Jones RG, Lee RW, Rowell DP (2015) Selecting CMIP5 GCMs for downscaling over multiple regions. Clim Dyn 44:3237–3260

MEMEE (2009) Stratégie Nationale de l'Eau. Ministère de l'Energie, des Mines, de l'Eau et de l'Environnement

Milewski A, Elkadiri R, Durham M (2015) Assessment and comparison of TMPA satellite precipitation products in varying climatic and topographic regimes in Morocco. Remote Sens 7:5697–5717

Pal JS et al (2007) Regional climate modeling for the developing world: the ICTP RegCM3 and RegCNET. Bull Am Meteorol Soc 88:1395–1409

Pal JS, Small EE, Eltahir EAB (2000) Simulation of regional-scale water and energy budgets: representation of subgrid cloud and precipitation processes within RegCM. J Geophys Res 105:29579–29594

Pal JS, Eltahir EAB (2016) Future temperature in southwest Asia projected to exceed a threshold for human adaptability. Nature Clim Change 6:128–129

Pepin N et al (2015) Elevation-dependent warming in mountain regions of the world. Nat Clim Change 5:424–430

Prein AF et al (2015) A review on regional convection-permitting climate modeling: demonstrations, prospects, and challenges. Rev Geophys 53:323–361

Rangwala I, Miller JR (2012) Climate change in mountains: a review of elevation-dependent warming and its possible causes. Clim Change 114:527–547

Reynolds RW, Rayner NA, Smith TM, Stokes DM, Wang W (2002) An improved in situ and satellite SST analysis for climate. J Clim 15:1609–1625

Romera R, Sánchez E, Domínguez M, Gaertner MA, Gallardo C (2015) Evaluation of present-climate precipitation in 25 km resolution regional climate model simulations over Northwest Africa. Climate Res 66(2):125–139

Seager R, Liu H, Henderson N, Simpson I, Kelley C, Shaw T, Kushnir Y, Ting M (2014) Causes of increasing aridification of the Mediterranean region in response to rising greenhouse gases. J Climate 27:4655–4676

Solman S, Nuñez M, Cabre MF (2008) Regional climate change experiments over southern South America. I: present climate. Clim Dyn 30:533–552

Stéfanon M et al (2014) Soil moisture-temperature feedbacks at mesoscale during summer heat waves over Western Europe. Clim Dyn 42:1309–1324

Taylor KE, Stouffer RJ, Meehl GA (2012) An overview of CMIP5 and the experiment design. Bull Am Meteorol Soc 93:485–498

Tebaldi C, Smith RW, Nychka D, Mearns LO (2005) Quantifying uncertainty in projections of regional climate change: a Bayesian approach to the analysis of multi-model ensembles. J Clim 18:1524–1540

Tramblay Y, Ruelland D, Somot S, Bouchaia R, Servat E (2013) High-resolution Med-CORDEX regional climate model simulations for hydrological impact studies: a first evaluation of the ALADIN-Climate model in Morocco. Hydrol Earth Syst Sci 17:3721–3739

Tramblay Y, Jarlan L, Hanich L, Somot S (2018) Future scenarios of surface water resources availability in north African dams. Water Resour Manage 32:1291–1306

Tuel A, Eltahir EAB (2020) Why is the Mediterranean a Climate Change Hotspot? Accepted in Journal of Climate

Van Vuuren DP et al (2011) The representative concentration pathways: an overview. Climatic Change 109:5–31

Walton DB, Hall A, Berg N, Schwartz M, Sun F (2017) Incorporating snow albedo feedback into downscaled temperature and snow cover projections for California's sierra Nevada. J Climate 30:1417–1438

Wang X, Li J, Sun C, Liu T (2017) NAO and its relationship with the Northern Hemisphere mean surface temperature in CMIP5 simulations. J Geophys Res Atmos 122:4202–4227

Winter JM, Pal JS, Eltahir EAB (2009) Coupling of integrated biosphere simulator to regional climate model version 3. J Clim 22:2743–2757

Zappa G, Hoskins BJ, Shepherd TG (2015) The dependence of wintertime Mediterranean precipitation on the atmospheric circulation response to climate change. Environ Res Lett 10:104012

Zeng X, Zhao M, Dickinson RE (1998) Intercomparison of bulk aerodynamic algorithms for the computation of sea surface fluxes using TOGA COARE and TAO data. J Climate 11:2628–2644